J Physiol 587.21 (2009) pp 5081–5093

The Journal of Physiology

Differential expression of membrane conductances underlies spontaneous event initiation by rostral midline neurons in the embryonic mouse hindbrain

Audrey M. Moruzzi, Nauzley C. Abedini, Matthew A. Hansen, Julia E. Olson and Martha M. Bosma

Department of Biology, University of Washington, Seattle, WA 98195-1800, USA

Spontaneous activity is expressed in many developing CNS structures and is crucial in correct network development. Previous work using $[Ca^{2+}]_i$ imaging showed that in the embryonic mouse hindbrain spontaneous activity is initated by a driver population, the serotonergic neurons of the nascent raphe. Serotonergic neurons derived from former rhombomere 2 drive 90% of all hindbrain events at E11.5. We now demonstrate that the electrical correlate of individual events is a spontaneous depolarization, which originates at the rostral midline and drives events laterally. Midline events have both a rapid spike and a large plateau component, while events in lateral tissue comprise only a smaller amplitude plateau. Lateral cells have a large resting conductance and are highly coupled via neurobiotin-permeant gap junctions, while midline cells are significantly less gap junction-coupled and uniquely express a T-type Ca^{2+} channel. We propose that the combination of low resting conductance and expression of T-type Ca^{2+} current is permissive for midline neurons to acquire the initiator or driver phenotype, while cells without these features cannot drive activity. This demonstrates that expression of specific conductances contributes to the ability to drive spontaneous activity in a developing network.

(Received 9 August 2009; accepted after revision 2 September 2009; first published online 7 September 2009)
Corresponding author M. M. Bosma: Department of Biology, University of Washington, Seattle, WA 98195-1800, USA. Email: martibee@u.washington.edu

Abbreviations DRN, dorsal raphe nucleus; InZ, initiation zone; SA, spontaneous activity; SPA, synchronous plateau assembly; r, rhombomere; VII, facial; V, trigeminal; 5HT, serotonin; E, embryonic; $[Ca]_i$, intracellular calcium.

Introduction

During embryonic development, the vertebrate hindbrain is transiently segregated into rhombomeres, which influence neuronal fate determination and organization (Lumsden & Keynes, 1989; Lumsden, 1990; Guthrie, 1996). In mice, rhombomeres (r) are present from embryonic day (E)8 to E11.5. Cranial nerve nuclei develop around E9–E10, including the trigeminal (V), originating in r2 and r3, and the facial (VII), originating in r4 and r5. The hindbrain also contains neurons of the developing serotonergic system, which begin to differentiate at E11.5 in former r1–r3, representing the future rostral-innervating raphe nuclei; at E12.5, a second group of serotonergic cells, which innervate the spinal cord in the adult, appears more caudally in the former r5–r7 region (Wallace & Lauder, 1983; Hendricks *et al.* 1999). At E11.5, 80% of neurons within the former r1–r3 and within 125 μm of the midline are immuno-positive for serotonin (Hunt *et al.* 2005).

We have previously used $[Ca]_i$ imaging to show that spontaneous activity (SA) appears at E9.5 in hindbrain motor neurons, and becomes highly synchronized throughout the hindbrain by E11.5 (Gust *et al.* 2003). At E11.5, synchronized activity originates from rostral midline neurons within the former r2, and propagates laterally, rostrally and caudally throughout the hindbrain. These initiator neurons of the rostral midline hindbrain also send activity rostrally across the isthmus, driving SA throughout the midbrain (Rockhill *et al.* 2009). Between E11.5 and E13.5, SA retracts from lateral hindbrain, and then from more rostral and caudal midline sites to only the former r2 pacemaker, before ceasing completely by E14.5 (Hunt *et al.* 2006*b*).

The electrophysiological mechanisms that underlie the driver function of rostral midline neurons of the hindbrain have not been characterized. Previous work has shown that synchronized SA, as recorded using $[Ca^{2+}]_i$ imaging, is blocked by antagonists at the $5HT_{2A/C}$ receptor, and that at E11.5 no other transmitter systems are required for SA

DOI: 10.1113/jphysiol.2009.180091

(Hunt *et al.* 2006*a*). SA is also suppressed by gap junction blockers and augmented by ammonium, which transiently opens gap junction channels (Hunt *et al.* 2006*a*), suggesting a role for gap junctions in SA.

In the present experiments, we asked what electrophysiological properties distinguish driver midline from lateral cells in the rostral hindbrain. We show that midline neurons express spontaneous depolarizations with an initial spike and a slower plateau, which comprise the electrical basis of SA observed using $[Ca^{2+}]_i$ imaging. Lateral cells have depolarizations that lack the spike component and have smaller plateaus. Medial neurons also have significantly higher resistance, possibly due to less gap junction-mediated coupling than lateral cells, and additionally express a transient inward current, which is sensitive to Ni^{2+} and insensitive to TTX. It therefore appears that a combination of low gap junctional coupling, high resistance and transient (T-type) Ca^{2+} currents confer initiator ability on rostral midline neurons of the developing hindbrain.

Methods

Tissue preparation

Timed-pregnant E11.5 Swiss/Webster mice (E0.5 defined as the morning of plug formation) were acquired from Harlan Laboratories (Livermore, CA, USA), kept for 1–5 days in conditions of standard lighting and with enrichment, and killed by an excess of CO_2 followed by cervical dislocation, all in accordance with the regulations of the University of Washington Animal Care Committee (IACUC) and the ethics policy of *The Journal of Physiology* (Drummond, 2009). All efforts were made to minimize suffering by the animals, to minimize the number of animals used, and to use all embryos obtained from each female. Embryos were removed from uteri into carbogen (95% O_2–5% CO_2)-bubbled ACSF, containing (in mM): 119 NaCl, 2.5 KCl, 1.3 $MgCl_2$, 2.5 $CaCl_2$, 1.0 NaH_2PO_4, 26.2 $NaHCO_3$, 11 glucose. The hindbrains were dissected out and cleaned of mesenchyme; a cut was made along the dorsal midline and the tissue placed in the open-book configuration on the stage of an inverted microscope. All experiments were performed at approximately 25°C. All values are presented as the mean and standard error of the mean (S.E.M.).

Electrophysiology and $[Ca^{2+}]_i$ imaging

Whole-cell recordings of midline neurons were made with patch electrodes (5–15 MΩ) filled with either K^+- or Cs^+-based intracellular solution with 10 mg ml^{-1} neurobiotin. The K^+-based solution contained (in mM): 100 potassium gluconate, 0.5 EGTA, 5 $MgCl_2$, 40 Hepes, 3 Na-ATP, 3 Na-GTP, pH 7.25; the Cs^+-based solution contained (in mM): 95 $CsMeSO_4$, 10 CsCl, 1 EGTA, 5 $MgCl_2$, 40 Hepes, 3 Na-ATP, 3 Na-GTP, pH 7.25. All cells were recorded in voltage-clamp mode initially, followed by current-clamp. Signals were recorded with an Axopatch 200B patch clamp (Axon Instruments/Molecular Devices, Sunnyvale, CA, USA). Data were acquired and pulses generated using Axoclamp software (Axon Instruments/Molecular Devices), filtered at 333 Hz and digitized at a 1 kHz sampling frequency. Recordings using the two solutions were corrected for junction potentials measured separately. Calcium currents were expressed as densities; cell size in picofarads was measured using the resultant voltage transient at the transition point of an applied triangle wave. In the conductance experiments, ramps were leak-subtracted by the averaged values of current recorded during ± 15 mV steps from the resting potential.

For simultaneous whole-cell patch and $[Ca^{2+}]_i$ imaging experiments, hindbrains were first bubbled in ACSF containing 1.75 μM of the $[Ca^{2+}]_i$ indicator dye fluo-4 and 0.07% Pluronic-127 (Molecular Probes/Invitrogen, Carlsbad, CA, USA) for 15 min. Once loaded, the tissue was positioned in the open-book preparation in a microscope chamber and imaged on a Nikon Diaphot inverted microscope (Nikon Instruments, Melville, NY, USA) or Zeiss upright Axioskop microscope (Carl Zeiss, Thornwood, NY, USA) with a cooled CCD camera (Photometrics, Pleasanton, CA, USA) at 0.3 Hz (10 Hz for rapid acquisition). The chamber was constantly perfused with carbogen-bubbled ACSF at a rate of 1 ml min^{-1}. Images and measurements were recorded using MetaFluor (Universal Imaging/Molecular Devices, Downington, PA, USA) and subsequently analysed using MetaFluor Analyst, SigmaPlot (Systat, San Jose, CA, USA), Microsoft Excel 2003, ImageJ (NIH, Bethesda, MD, USA) and Adobe Photoshop. The gradual baseline decline in $[Ca^{2+}]_i$ imaging traces is due to photobleaching. The initiation zone (InZ) was identified by frequency and direction of events; electrode positioning was made relative to the InZ, and confirmed in confocal microscopy after reacting the neurobiotin that filled the cells. Pharmacological agents were diluted in carbogen-bubbled ACSF before application. Ketanserin, mefloquine, mibefradil, ZD7288 and E4031 were from Tocris Bioscience, Ellisville, MO, USA; nickel chloride was from Sigma, St Louis, MO, USA.

Neurobiotin and immunocytochemistry

In hindbrains examined for cell coupling, reaction for neurobiotin was performed after dissected hindbrain fixation in 4°C freshly made 4% paraformaldehyde in phosphate buffered saline (PBS) containing (in mM): 3.16 NaH_2PO_4, 6.84 Na_2HPO_4, 150 NaCl, pH 7.2. Tissue was

incubated for 24 h with 1 : 1000 streptavidin conjugated to Alexa-594 (Molecular Probes/Invitrogen, Carlsbad, CA, USA). In some experiments, the fluorescent DNA marker 4′6-diamidino-2-phenylindole hydrochloride (DAPI) was applied at 1 : 1000 in PBS for 10 min. Tissue was examined using a Bio-Rad confocal microscope (Bio-Rad, Hercules, CA, USA); initial counting of cluster size (neurobiotin-filled cells) utilized confocal images taken at 400×, and whole-hindbrains were re-imaged at 100× to determine neuron position relative to identified axes. Number of cells was counted up to 50; larger clusters could not be counted accurately and were assigned the value of 50. Images were readied for analysis and publication with Adobe Photoshop.

For immunocytochemistry, hindbrains or whole embryos were dissected in ACSF and then fixed at 4°C in freshly made 4% paraformaldehyde in PBS for 3 h. Embryos were cryoprotected in 20% sucrose in PBS overnight, embedded and frozen in Optimal Cutting Temperature (OCT) medium (Electron Microscopy Sciences, Hatfield, PA, USA), and sectioned at 25 μm in a cryostat at –22°C. Immunocytochemistry (ICC) was performed in PBS containing 0.3% Triton X-100. Tissue was blocked at 4°C for 1 h with 10% normal goat serum (Jackson ImmunoResearch Laboratories, West Grove, PA, USA) and incubated with primary antibodies at 4°C for 72 h. Primary antibodies were rabbit anti-5HT (ImmunoStar, Hudson, WI, USA) and rabbit anti-$Ca_v3.3$ (Alomone Laboratories, Jerusalem, Israel). Negative controls without antibody showed no signal when examined in the confocal microscope; for $Ca_v3.3$, controls with antigen (supplied with antibody) pre-absorbed showed no signal. Appropriate secondary antibodies (Alexa 488 or 594; Molecular Probes/Invitrogen, Carlsbad, CA, USA) were applied for 1 h at 4°C. Sections were examined and photographed with a Bio-Rad confocal microscope and images readied for analysis and publication with Photoshop and ImageJ.

Results

Spontaneous activity (SA) in the mouse hindbrain originates within an initiation zone (InZ) derived from the former r2 in the rostral midline (Hunt *et al.* 2006*a*). We previously showed that at E11.5 all serotonergic neurons are located within 125 μm of the midline, and that more than 80% of the neurons within the InZ are 5HT-positive (Hunt *et al.* 2005). Using patch clamp techniques, we compared neurons within the InZ to those in lateral follower regions to ascertain the specific electrophysiological characteristics that determine the ability of midline InZ cells to initiate spontaneous activity.

We first confirmed, using simultaneous whole-cell recording and $[Ca^{2+}]_i$ imaging, that the spontaneous electrical events that we record underlie $[Ca^{2+}]_i$ events. $[Ca^{2+}]_i$ events were recorded from regions that included approximately 30 neurons. Each $[Ca^{2+}]_i$ event from regions overlying the recording site was accompanied by an electrical event, and frequencies of electrical events and $[Ca^{2+}]_i$ events were similar at different sites within the hindbrain. Within 200 μm of the midline, less than 1% of the electrical events were uncorrelated with $[Ca^{2+}]_i$ events; between 100 and 400 μm of the midline, the frequency of both electrical and $[Ca^{2+}]_i$ events dropped off linearly ($n = 10$) (range 3.2–0.5 min^{-1}). No consistent relationship in amplitude or spike duration was found between these two phenomena (analysed in 5 simultaneous recordings); thus, as shown in Fig. 1*A*, smaller voltage events did not always mediate smaller $[Ca^{2+}]_i$ events. This suggests that each $[Ca^{2+}]_i$ and voltage event may include contributions from overlapping and variable interactions between neighbouring neurons.

Spontaneous electrical events differ dramatically from classic action potentials: the events are graded and vary in amplitude and duration, on some occasions even within the same cell; the potential does not consistently overshoot 0 mV; and events are several orders of magnitude slower than conventional action potentials (100–1500 ms in duration).

By using simultaneous dual patch recordings, we determined that electrical events originate in regions near the midline, and propagate to more lateral regions (Fig. 1*B*; $n = 4$), similar to the midline initiation and lateral propagation observed in $[Ca^{2+}]_i$ imaging. This suggests that each event is derived from a midline source and is consistent with events originating medially, propagating to lateral cells. The electrical events had varying amplitudes and temporal characteristics in medial *vs.* lateral cells, and we demonstrate below that these characteristics correlate with specific hindbrain positions. In addition, events from more caudal sites invariably lag those from rostral sites, again showing that rostral sites initiate events (Fig. 1*C*; $n = 2$).

We recorded from neurons from different sites in the hindbrain, using pipettes containing neurobiotin to mark cell positions, which were then compared to specific anatomical landmarks. These landmarks included the 5HT-positive neurons in fixed immunostained E11.5 hindbrains (Fig. 2*A*, left panel), or Pet1-YFP-labelled neurons (Fig. 2*A*, right panel). 5HT is expressed continually as the serotonergic neurons differentiate and migrate to the marginal zone from the ventricular zone (Hunt *et al.* 2005). The Pet-1 promoter is transiently expressed upon withdrawal from the cell cycle in 70% of all 5HT-positive neurons (Hendricks *et al.* 2003). At E11.5, the rostral group of 5HT/Pet-1-expressing cells extends from the isthmus (midbrain-hindbrain boundary) to the rostral end of former rhombomere 4 (r4). The caudal serotonin group (caudal to the posterior border

of r4) is not yet expressing Pet-1 or 5HT at E11.5. Additional landmarks were the trigeminal (Vth) and facial (VIIth) motor neurons retrogradely identified with Texas Red-labelled dextran (Fig. 2*B*). The cell bodies of the Vth cranial nerve are found laterally within former r2/r3, while the axons exit laterally in former r2; the cell bodies of the VIIth cranial nerve migrate to former r6, while the axons exit the hindbrain laterally within former r4; the trajectory of the VIIth axons is seen running rostrally next to the midline. Recorded sites were measured relative to the isthmus and the midline, and electrophysiological properties from each recorded neuron were plotted onto a map of the hindbrain (Fig. 2*C*). In the rostrocaudal axis, all of the recorded sites are referenced to the isthmus between the hindbrain and midbrain, which is designated as 0 μm. In the mediolateral axis, the scale is expanded for clarity, and all sites are plotted relative to the midline of the floor plate. In the open-book configuration, the opening of the hindbrain constrains the 5HT-positive neurons into a slightly more medial position, to within 100 μm of the midline.

Electrical events are larger and biphasic in medial cells

The resting membrane potential (V_m) of the cells averaged -53 ± 1.03 mV ($n = 87$), and did not vary significantly with the position of the cell within the hindbrain (medial neurons: -52.9 ± 1.3 mV ($n = 69$); lateral neurons: -57.4 ± 2.44 mV ($n = 18$); $P = 0.11$). Cells in which V_m was positive to -44 mV were excluded from further analysis. If needed, cells were held more negative than -50 mV by applying 1–2 pA of holding current; cells which required more holding current were excluded from analysis. The averaged maximal amplitudes of the first three to five events in current clamp recordings from each of 87 neurons (examples shown as insets in Fig. 2*C*) are

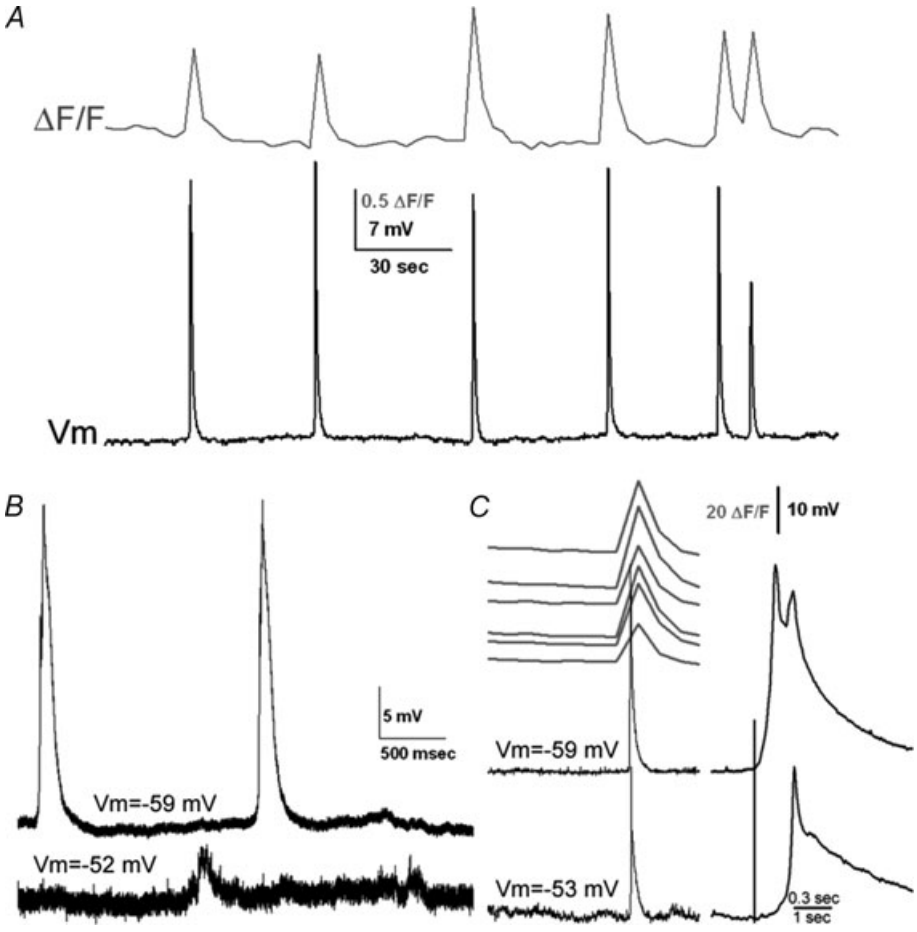

Figure 1. Electrical events are correlated temporally with $[Ca^{2+}]_i$ events
A, in simultaneous $[Ca^{2+}]_i$ imaging and current clamp recording from neurons in the InZ, single $[Ca^{2+}]_i$ events correlate with spikes in electrical events. Resting potential for this cell = -57 mV. *B*, dual recording from cells approximately 120 μm apart, medial to lateral; the estimated propagation rate of the event is 1066 μm s^{-1}. *C*, simultaneous $[Ca^{2+}]_i$ imaging of midline regions and dual patch recording; cell recorded in the bottom trace was approximately 50 μm caudal to the cell in the top trace. Expanded traces, on right, show details of the waveforms of the events. Potassium gluconate pipette solution.

plotted on medio-lateral and rostro-caudal axes of the grid of the hindbrain; the diameter of each circle on the grid represents the maximal total amplitude (see measurement in Fig. 2*D*) of the events recorded from that cell. Because the range of total event amplitudes was large (1–74 mV), diameters are plotted on a logarithmic scale to allow visualization of the very small lateral events. The data show that events in the midline region are larger than those in lateral regions.

The shapes of the depolarizing events also vary by region, as shown by insets in Fig. 2*C*. Some events have a rapid initial spike riding on a slower plateau and thus have a deflection in the falling phase of the event (biphasic events), while other events have only the slower plateau. We analysed the two phases of the events separately, measuring peak amplitude and half-duration for each, as exemplified by the analysis of the event in Fig. 2*D*. Each event was then categorized by those parameters, and by position on the hindbrain, to clarify differences between midline and lateral neurons. As shown in Fig. 3*A*, the shorter-duration spike component of the event was found only in neurons located within 100 μm of the midline (open circles), and had a mean amplitude of 13.3 ± 1.30 mV ($n = 43$). (Some spike components had multiple peaks, e.g. top inset in Fig. 2 and Fig. 1*C*; in these cases, only the first spike was measured.)

Although the slower plateau was a component of all events, it was larger near the midline (18.97 ± 1.20 mV; $n = 69$ *vs.* 2.0 ± 0.60 mV; $n = 18$; $P = 0.0006$; Fig. 3*A*, grey circles; Fig. 3*B*). Cells > 500 um from the midline

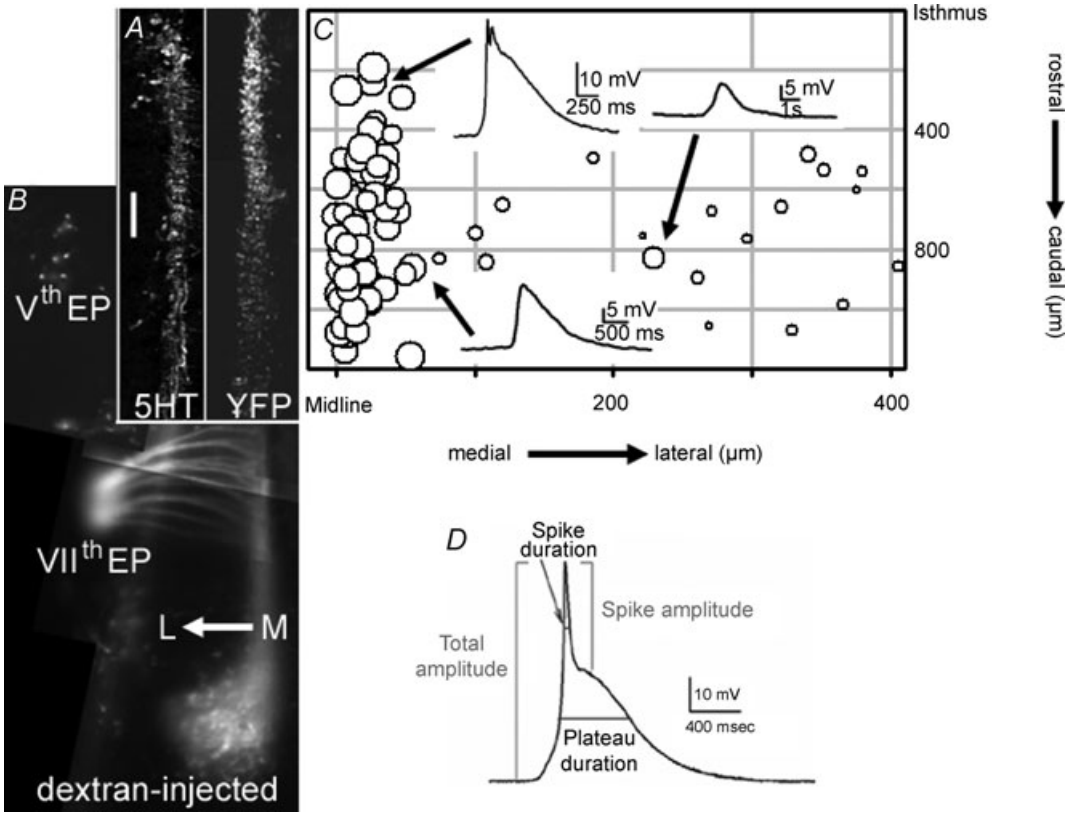

Figure 2. Event properties and amplitudes vary with medio-lateral position
A, left panel: fixed hemi-hindbrain, sliced in the coronal plane to emulate the open-book preparation, showing extent of 5HT-positive neurons in the rostral serotonergic raphe group from the isthmus (midbrain-hindbrain junction) to the rostral border of former r4. Right panel: YFP-Pet1-labelled neurons in coronal hemi-hindbrain section, showing the rostral–caudal extent of the Pet-1-positive cells. Scale bar = 200 μm. *B*, dextran injection into branchial arches b1 and b2 demonstrates the Vth nerve (in the former r2) and the fan of the VIIth nerve (exit point is in former r4) in live hindbrain. Line of medial-lateral arrow is 200 μm. *C*, events are plotted as symbols against rostrocaudal and mediolateral position; symbol diameter represents the logarithm of the maximal total amplitude of each event. Insets show events from indicated sites (arrows). Events at the midline are larger and often have both a spike and a plateau. Potassium gluconate pipette solution. *A*, *B* and *C* are shown to the same vertical (rostrocaudal) scale, with the isthmus as the 0 μm point; horizontal (mediolateral) scale in *C* is expanded for clarity, with the midline as the 0 μm point. *D*, measurement of event parameters. Total amplitudes were measured from the baseline to the maximal spike excursion; spike amplitudes were measured from the top of the plateau to peak of total event; plateau amplitude was the difference between those values. Duration of each component was measured at the half-amplitude point.

showed no discernible events ($n = 9$), despite having resting potentials not distinguishable from more medial cells (−45 to −58 mV). Lateral neurons also had longer duration events than medial neurons (700.6 ± 45.7 ms ($n = 69$) *vs.* 1539.0 ± 176.0 ms ($n = 18$); $P < 0.007$) (Fig. 3*C*, hatched bars).

In order to ascertain the role of K^+ currents in event shape and kinetics we characterized events using pipettes that contained $CsMeSO_4$. Events with Cs^+-pipettes had a very similar distribution to those with a K^+-containing pipette: near the midline, biphasic events (spike and plateau) were observed, while only plateau-containing events were found lateral to 100 μm. The amplitude distribution of medial *versus* lateral event plateaus was very similar to that recorded with K^+-filled pipettes (Cs^+: medial 19.6 ± 2.48 mV, $n = 25$, range 3.0–53.0 mV; lateral 2.7 ± 1.03 mV, $n = 23$, range 0.5–24.0 mV; Fig. 3*B*, hatched bars). Surprisingly, the durations of the plateaus were also similar to those observed in K^+-filled pipettes (Cs^+: medial 831.1 ± 166.5 ms; lateral 1467.9 ± 277.9 ms) (Fig. 3*C*, hatched bars), suggesting that K^+ currents do not contribute significantly to the falling phase of the plateau. However, the amplitudes of the midline spikes were significantly larger (22.42 ± 3.7 mV, range = 8.0–40.0 mV,

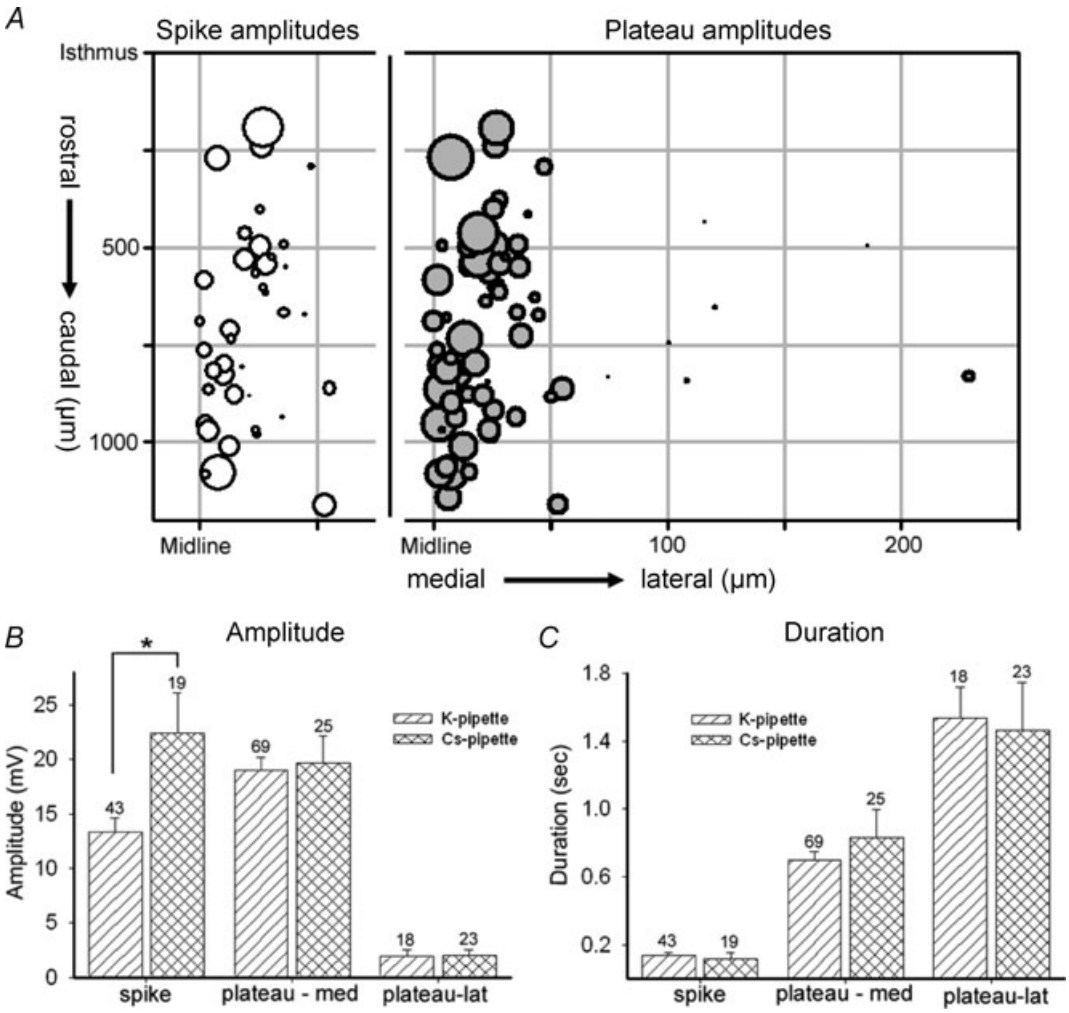

Figure 3. Summary analysis of event parameters
A, double-plot of the isolated amplitudes of spike (left) or plateau (right) events, against position. The *x*-axis is replicated at left for the midline–100 μm range to plot only the spike components (open circles), found only within 100 μm of the midline; plateau components (grey circles) are plotted on the 0–250 μm range, as they are recorded medially and laterally in the hindbrain. Potassium gluconate pipette solution. *B* and *C*, distribution of different components of depolarizing events, comparing data derived from K^+- and Cs^+-filled pipettes. *B*, the amplitudes of plateau components were similar in both pipette solutions, with lateral plateaus being significantly smaller than those recorded from medial cells. The amplitude of the spike component, however, was significantly larger in recordings using Cs^+-filled pipettes (asterisk; $P < 0.0016$). *C*, the duration of all components was the same when measured with K^+- or Cs^+-filled pipettes; medial plateau durations (middle columns) are significantly shorter than those recorded in lateral cells (right columns).

$n = 19$) (Fig. 3*B*, first pair of columns, hatched bars). Half-width durations of spikes between the two solutions was not significantly different Cs^+: 116.6 ± 37.0 ms; K^+: 138.9 ± 14.2 ms (Fig. 3*B*, first pair of columns). These data indicate that K^+ currents may impede the full depolarization of the rapid spike, but the plateau phase of the depolarizing events is independent of K^+ conductances.

Gap junctional coupling is involved in propagation of events

We next asked whether gap junctional coupling was involved either in the initiation of SA or in propagation of events from medial to lateral regions. Earlier experiments in mouse hindbrain showed that applying the somewhat nonspecific gap junction blockers octanol or heptanol blocked SA (Hunt *et al.* 2006*a*). The antimalarial agent, mefloquine, has been shown to be relatively specific in blocking gap junctions made up of Cx36 and Cx50 (Cruikshank *et al.* 2004). Application of $100\,\mu$M mefloquine irreversibly inhibited spontaneous $[Ca^{2+}]_i$ events in hindbrain (not shown; $n = 4$). At a concentration of $10\,\mu$M, four preparations showed a significant decrease in frequency of events, to $36 \pm 14\%$ ($P < 0.01$).

These data suggest that one mechanism by which the events in lateral tissue may be both smaller and slower is that lateral neurons may be more extensively gap junction coupled than in the midline tissue. However, it is also possible that a low level of gap junctional coupling may play a role in the initiation of events in the InZ. To test differential gap junction expression, we measured the number of cells which were labelled by neurobiotin after recording from one neuron for a fixed duration, and compared the neurobiotin-coupled cluster size at different hindbrain positions. Figure 4*Aa* and *b* are images of clusters of neurobiotin-coupled neurons, obtained at 400× in a confocal microscope, showing multiple neurobiotin-positive cells coupled to the single recorded neuron. Figures 4*B* and *C* show examples of both amplitude and cluster size for three cells recorded from the same hindbrain, to compare the medio-lateral distribution of neurobiotin coupling. The current clamp traces show that medial neurons have larger events, which are more likely to contain spike components, while the 100× confocal images show that lateral recordings had greater neurobiotin-coupled cluster size. Confocal images taken at 400× were used to count the number of cells in each neurobiotin-coupled cluster, and the cluster sizes plotted against hindbrain position (Fig. 4*E*). Midline cells had a cluster size of 8.42 ± 0.74 cells ($n = 69$), while the cluster size outside of the $100\,\mu$m boundary was 24.3 ± 3.4 cells ($n = 24$; $P = 0.006$) (Fig. 4*D*). Thus, lateral tissue is significantly more coupled via neurobiotin-permeant gap junctions than is the midline tissue.

In order to characterize the relationship between cluster size and electrophysiological properties, and to test the hypothesis that decreased coupling correlates with decreased leak conductance (and higher excitability), we examined the spatial variation of resting linear leak conductance by measuring current responses to an applied ramp in voltage clamp recording. Figures 5*Aa* and *Ba* show examples of hindbrains from which multiple cells were recorded, followed by *post hoc* examination of cluster size. As shown previously, cells nearer the midline have larger amplitude, and often biphasic, events. In addition, upon reacting the hindbrains against the neurobiotin, medial cells had smaller cluster sizes. As shown in Fig. 5*Ab* and *Bb*, cells in more lateral regions of the hindbrain showed large linear responses to a voltage ramp from −110 to +30 mV (grey traces), while medial cells showed lower resting conductance and a discontinuity in the slope of the line at approximately −40 to −30 mV (black traces). When cells were analysed by position (Fig. 5*D*), leak conductance was significantly lower in medial than in lateral neurons (Fig. 5*C*; medial: 1.23 ± 0.10 nS; $n = 84$; lateral: 4.7 ± 0.35 nS; $n = 31$; $P < 0.000001$). This is most likely to be a consequence of the higher gap junctional coupling, and would have the effect of increasing the ability of midline neurons to initiate electrical events compared to lateral neurons.

Ca^{2+} channels are expressed in medial cells. Earlier experiments demonstrated that SA in mouse hindbrain requires external Ca^{2+}. To characterize inward Ca^{2+} currents, we performed voltage-clamp with Cs^+ in the pipette, which showed an inward current that activates at −45 mV, peaks at −35 mV, and has inactivating kinetics resembling the T-type Ca^{2+} channel (Fig. 6*A*). This current, $I_{Ca\text{-}T}$, is expressed only in medial cells; the mean current density of cells within $100\,\mu$m of the midline was -22.5 ± 1.6 pA pF^{-1} ($n = 68$). Lateral cells express no inward currents. The presence of $I_{Ca\text{-}T}$ in medial cells may underlie the rapid spike phase of spontaneous events, which is likely to be required for the initiation of SA. We also examined the localization of $Ca_v3.3$ in the hindbrain using immunocytochemistry, and found that signal was highest in the region of 5HT-positive cell bodies, but not in the marginal zone immediately ventral to those cell bodies. In addition, it was heavily expressed in axons crossing beneath the floor plate of the hindbrain (Fig. 6*C* and *D*). Immunocytochemistry against $Ca_v3.1$ did not consistently show clear areas of expression.

To assess the role of T-type Ca^{2+} channels in SA, we applied mibefradil and low concentrations of Ni^{2+}, blockers specific to the Ca_v3 family (Lee *et al.* 1999;

Lacinová, 2004). Mibefradil (10 μM) reversibly inhibited SA in all preparations tested ($n = 7$; not shown). Ni^{2+} at 100 μM reversibly blocked SA in $[Ca^{2+}]_i$ imaging (Fig. 7*A*; $n = 6$), while 10 μM had no effect (reduction of $2 \pm 4\%$; $n = 3$). These experiments suggest that $Ca_v3.2$ Ca^{2+} channels do not play a role in hindbrain SA, as that molecular species is sensitive to lower micromolar concentrations of Ni^{2+} (Lee *et al.* 1999). In simultaneous $[Ca^{2+}]_i$ imaging and patch recordings, 100 μM Ni^{2+} blocked the spike component of depolarizing events (Fig. 7*A*, insets; Fig. 7*Da* and *b*, grey traces; $n = 7$). In contrast, application of 600 nM TTX blocked neither the SA recorded in $[Ca^{2+}]_i$ imaging ($n = 14$) nor the spike component of depolarizing events (Fig. 7*B*; $n = 6$), even after 20 min of application (although the spike did run down during that time). Similarly, in voltage clamp, inward currents elicited by voltage steps were reduced by 50 μM Ni^{2+} (Fig. 7*C*; $n = 4$), but were not blocked by 600 nM TTX (not shown). Thus, the inward currents found in medial cells that drive SA are a T-type Ca^{2+} channel; because of the relatively low sensitivity to Ni^{2+}, it is likely that the $Ca_v3.2$ channel is not involved. SA is not affected by blockers of L-type Ca^{2+} channels (nifedipine, 1 μM; $n = 3$; not shown), or blockers of N-type Ca^{2+} channels (ω-conotoxin GVIA, 1 μM, $n = 3$; not shown) (Miljanich & Ramachandran, 1995).

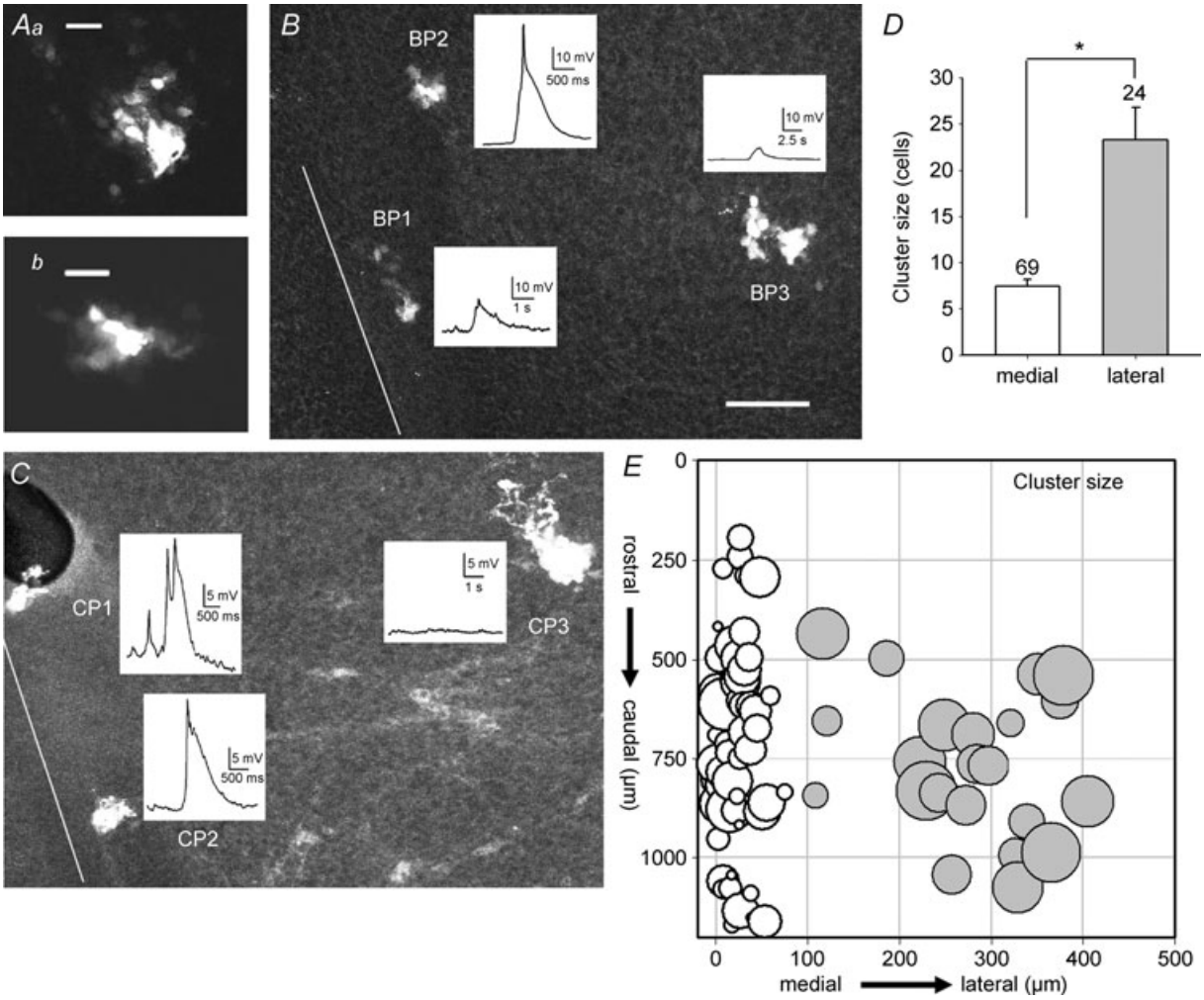

Figure 4. Cluster size, or number of neurobiotin-coupled neurons, is significantly larger in lateral positions

Aa and *b*, high power (400×) confocal images of clusters of neurobiotin-coupled neurons from medial positions. Scale bars are 10 μm. *B* and *C*, in each panel, low power (100×) confocal images of hindbrains with 3 recordings each are shown; neurons near the midline (white lines) have larger depolarizations and are coupled to fewer cells. Scale bar (30 μm) applies to both images. *D*, neurobiotin-coupled cluster size is significantly different between medial (white bar) and lateral (grey bar) positions. *E*, cluster size for each recorded neuron, counted in confocal images and plotted against position in the hindbrain, is shown on a logarithmic scale to facilitate better comparison. Each recording was held for 15 min, and the tissue fixed and reacted for neurobiotin. Potassium gluconate pipette solution.

Discussion

Spontaneous activity in the developing nervous system is crucial in correct network formation (for review see Moody & Bosma, 2005). SA can be elicited by synaptic or gap junctional coupling between cells in a network of connected elements or initiated by a discrete population of pacemaker elements driving other parts of the network. The embryonic mouse hindbrain is an example of a single region driving SA, with the midline serotonergic neurons initiating activity that then propagates throughout the hindbrain at E11.5 (Hunt *et al.* 2005). We show here that large biphasic pacemaker events, consisting of a rapid spike and slower plateau, are caused by electrophysiological properties found in the region containing the InZ (pacemaker region). These properties include higher input resistance secondary to less electrical coupling to neighbouring cells, allowing inputs to be initiated instead of dissipated and inward T-type currents that correlate with the ability to express the spike component of the events. In contrast, lateral neurons have high cluster number, indicating coupling to a larger number of cells, and express no inward currents.

Although these membrane parameters, including high resistance and T-type Ca^{2+} currents, have been shown to mediate spontaneous electrical activity in some adult pacemaker neurons (e.g. thalamus: Fuentealba & Steriade, 2005; Nelson *et al.* 2006), it is likely that some element of network connectivity is also needed for SA, as smaller pieces of hindbrain (either through transverse slicing or cutting the isolated InZ into pieces, not shown) are less likely to express SA. Sun & Luhmann (2007) have shown that cortical SA is not expressed in slices which are less than 1000 μm thick, another example where a critical mass of connectivity must be present for SA expression.

The electrical events recorded in the embryonic hindbrain are not typical of mature neuronal action potentials: they are graded in amplitude and do not always overshoot 0 mV; they have a relatively slow upstroke and are of very long duration. Thus, the spike component is longer than 100 ms, while the medial plateau component averages more than 500 ms and the lateral plateau more than 1500 ms in duration. This implies that the conventional complement of voltage-gated ion channels that mediate rapid all-or-none mature action potentials are not involved in these events. The spontaneous

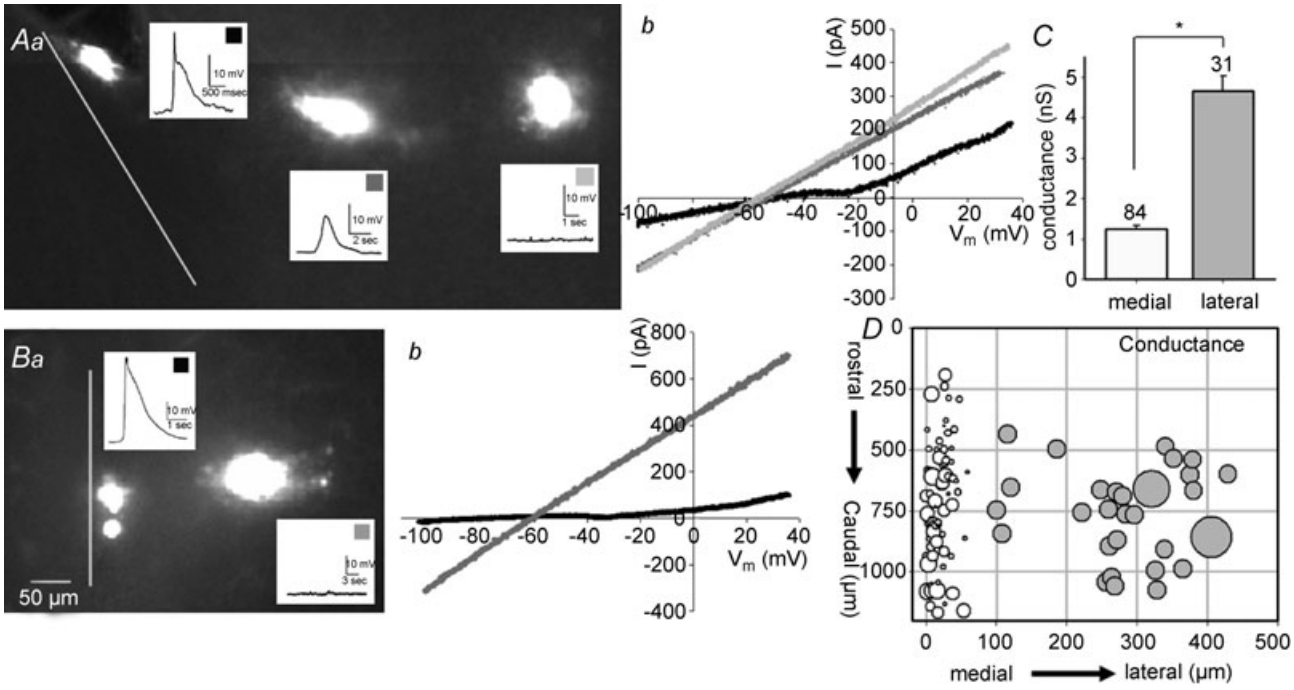

Figure 5. Neurons within 100 μm of the midline have high input resistance
A and *B*, examples of hindbrains with multiple recordings showing ramp voltage-clamp responses compared between medial and lateral cells. *Aa* and *Ba* are low power (100×) confocal images showing cell position, depolarizing events and neurobiotin coupling; scale bar of 50 μm applies to both images. *Ab* and *Bb* show resultant currents from ramps applied in voltage clamp; more lateral cells (shade of line corresponds to squares on insets) have higher resting conductance, reflected as steeper slope. Medial neurons in *A* and *B* express inward deflection in the slope of the resultant current at about −30 mV. *C*, conductance of all cells grouped by position show that lateral cells (grey bar) have significantly higher resting conductance than medial cells (white bar). *D*, the conductance (symbol size represents conductance), subtracted by leak, for each cell is plotted against position in the hindbrain, showing that lateral neurons have significantly higher resting conductance than those in medial positions. Potassium gluconate pipette solution.

depolarizing events are similar to action potentials elicited by stimulation in sea urchin oocytes, which have a biphasic shape, and are of similar durations (Okamoto *et al.* 1977; David *et al.* 1988). The depolarizing phases of the oocyte events are mediated by a T-type Ca^{2+} channel.

SA is recorded in a variety of neuronal structures, accompanied by large and sometimes slow depolarizations. In the neocortex, a sequence of distinct types of depolarizing potentials is recorded over the first postnatal week: after a period of random and asynchronous action potentials, approximately 1/3 of the neurons generate synchronous plateau assemblies (SPAs) which are not synaptically driven, but rely on Na^+ and L-type Ca^{2+} channels (Crepel *et al.* 2007 – hippocampus; Allene *et al.* 2008). These events closely approximate those recorded in mouse hindbrain, as they have single rapid components, long-duration (1–2 s) plateaus, and are blocked by gap junction inhibitors (Crepel *et al.* 2007). In contrast to those in hindbrain, there is reduction in their appearance with blockers of I_H. An additional contrast is demonstrated by the participation of only a small group of the homogeneous developing hippocampal neurons in SPAs, unlike the depolarizing events which encompass the entire midline of the hindbrain after midline initiation. SPAs in neocortex are developmentally replaced by synaptically driven early network oscillations (ENOs; driven by glutamate) and giant depolarizing potentials (GDPs – both hippocampus and cortex), which are driven by excitatory GABAergic input. Each of these includes a slow wave with overlying rapid bursts of activity; these are often preceded by synaptic inputs (Ben-Ari, 2001). SPAs may express $[Ca^{2+}]_i$ transients of a unique frequency and duration that differentially activate genes driving neuronal identity or phenotype, as they resemble those recorded in developing neurons of *Xenopus* spinal cord (Gu & Spitzer, 1993, 1995; Watt *et al.* 2000; Borodinsky *et al.* 2004). Similarly, the depolarizing events expressed in these very early hindbrain developmental stages may be crucial in phenotype specification.

Although the electrophysiological properties expressed in rostral midline cells, including the InZ, are permissive for initiation of depolarizing events leading to SA, they are not necessarily the only mechanisms required for that activity. Block of $5HT_{2A/C}$ receptors by ketanserin completely silences hindbrain SA at all stages where it is expressed (Hunt *et al.* 2006*a*). $5HT_{2A}$ receptors are

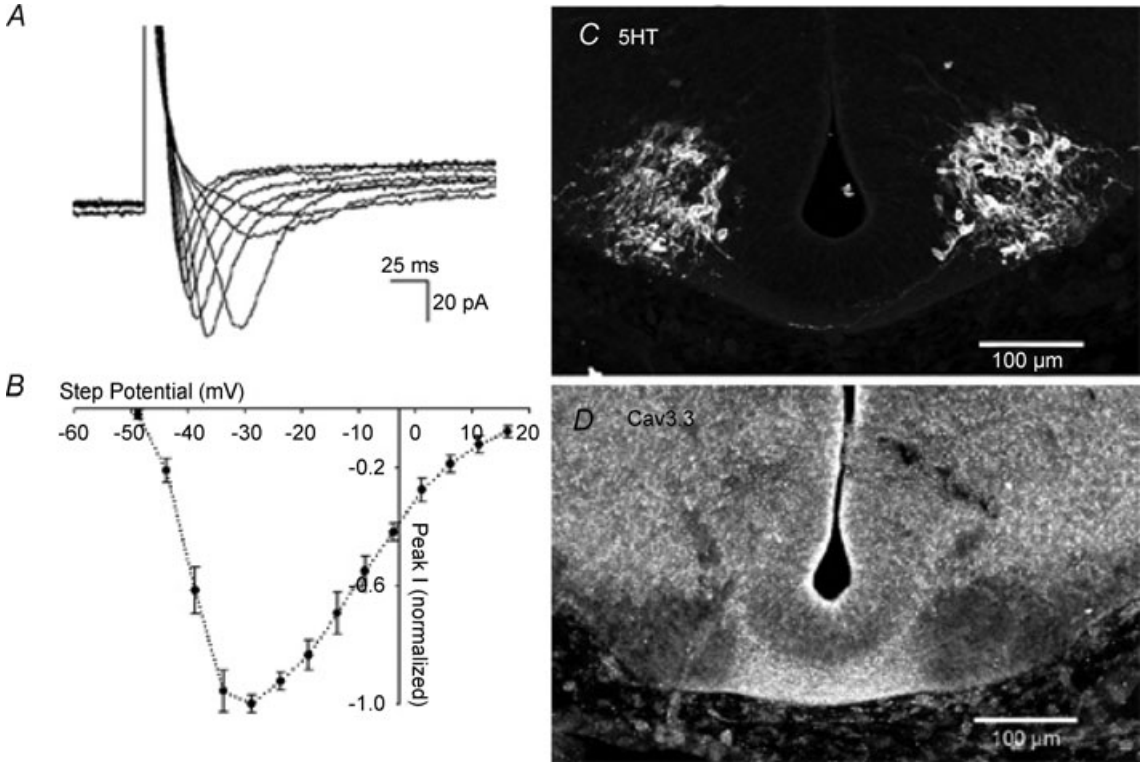

Figure 6. Characterization of T-type Ca^{2+} channels in medial hindbrain cells
A, inward currents recorded using Cs^+-filled pipette in voltage clamp during steps to −50 to −10 mV in 5 mV increments; holding potential was −95 mV. *B*, current–voltage relation for inward currents averaged from eight neurons, showing peak of inward current at approximately −35 mV. *C*, control panel shows transverse section of hindbrain using an antibody directed against 5HT. *D*, similar section in sibling E11.5 embryo, using an antibody against the $Ca_v3.3$ protein, showing strong staining in the region of 5HT-positive cell bodies and in the commissural region of crossing axons. $CsMeSO_4$ pipette solution.

expressed widely, both in lateral marginal tissue and in 5HT-positive InZ neurons (Hunt *et al.* 2005), suggesting that the action of these receptors is important in both initiation and propagation of signals. It is possible that minute-to-minute regulation of conductances, such as $I_{Ca\text{-}T}$ up-regulation by $5HT_2$ receptor activation, allows initiation of individual depolarizing events in the midline; 5HT regulation of multiple Ca^{2+} channel types as been shown in adult raphe neurons (see below).

The raphe modulates many brain structures and is involved in a wide range of complex behaviours and patterns such as sleep, circadian rhythms and mood (Jacobs & Azmitia, 1992). In the serotonergic neurons that make up the dorsal raphe nucleus (DRN), derived from the rostral hindbrain (Wallace & Lauder, 1983), rhythmic activity persists into adult life. 5HT-positive neurons have slow rhythmic activity, with a relatively broad action potential, and an interspike period that includes a long ($\tau = \sim$7.3 ms; Kirby *et al.* 2003) after-hyperpolarization, followed by a slow depolarization leading to the next spike (Aghajanian & Vandermaelen, 1982). The slow depolarization is postulated to be mediated, at least in part, by a low threshold, Ni^{2+}-sensitive Ca^{2+} current (Burlhis & Aghajanian, 1987). $5HT_{1A}$ receptors are expressed on DRN neurons, and their activation leads to hyperpolarization and a cessation of firing. This is likely to be due to the

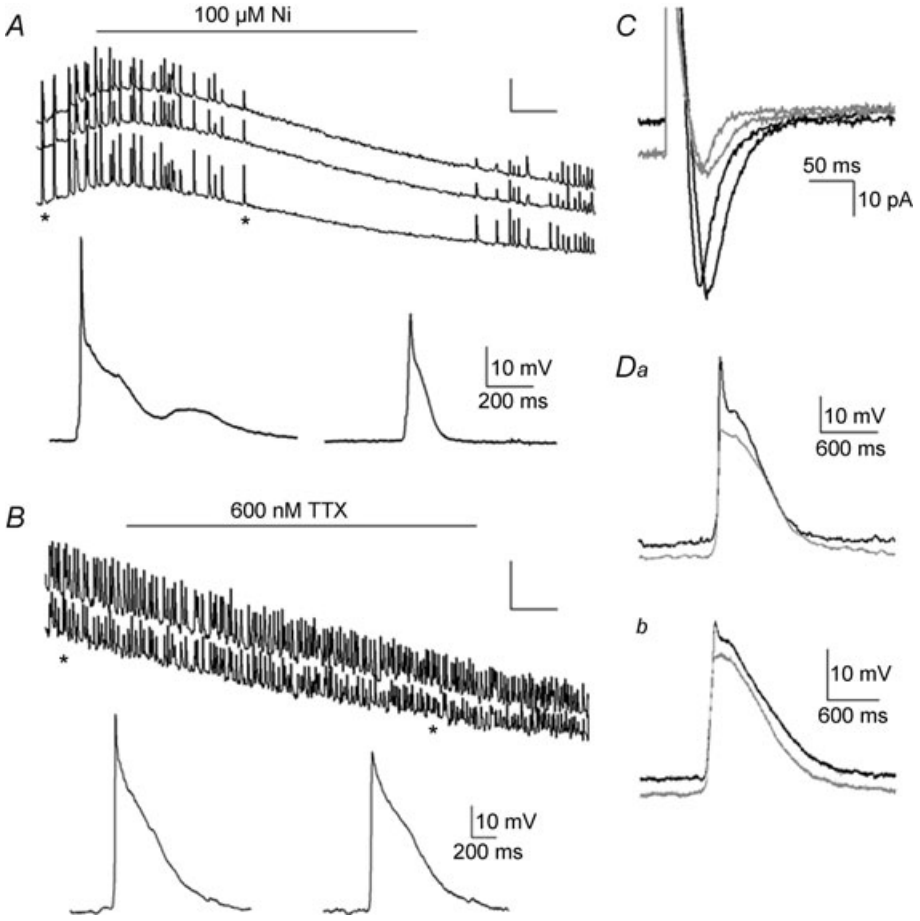

Figure 7. Blockers of $I_{Ca\text{-}T}$ abolish SA and the spike component of depolarizing events in medial hindbrain cells

A, simultaneous $[Ca^{2+}]_i$ imaging (top) and patch clamp of a medial neuron during application of 100 μM Ni^{2+}, which blocks SA. Asterisks show the time points where the expanded current clamp recordings of individual events are taken, which demonstrate that Ni^{2+} blocks the peak component of depolarizing events. *B*, simultaneous $[Ca^{2+}]_i$ (top) and patch recording during application of 600 nM TTX, which does not block SA in E11.5 midline neurons. Asterisks show the times at which individual expanded depolarizing events were recorded, showing that although the peak of the events decreases over time, it is not blocked by TTX. *C*, application of 50 μM Ni^{2+} during voltage clamp recoding of $I_{Ca\text{-}T}$ demonstrates reduction of that current (grey traces) by Ni^{2+}. *Da* and *b*, superposition of control (black) and Ni^{2+}-blocked (grey) depolarizing events in a medial (*Da*; 40 μm from midline) and more lateral (*Db*; 75 μm from midline) neuron demonstrate that application of 100 μM Ni^{2+} blocks the peak component of depolarizing events, but does not affect the plateau component. Events with Ni^{2+} are plotted slightly below the control traces for clarity; the resting potential did not change during the recordings. Potassium gluconate pipette solution (A,B,D); $CsMeSO_4$ pipette solution (C).

characteristic up-regulation of the inward rectifier current by 5HT stimulation (Penington *et al.* 1991, 1992, 1993; Pan & Williams, 1994). In fact, standard identification of mature 5HT raphe neurons is made by application of 5HT or M2 muscarinic agonists, causing an increase in IK_{IR} and cessation of activity (Pan & Williams, 1994; Bayliss *et al.* 1997*a*,*b*).

The expression of a transient, Ni^{2+}-sensitive Ca^{2+} channel in adult DRN implies a role for an inward current capable of participating in rhythmic or spontaneous activity during a range of maturation in these neurons. Later addition of other Ca^{2+} channel types may occur when network properties and synaptic inputs become established. In slightly later (E14) embryos, $Ca_v3.3$ is highly expressed along the midline of the hindbrain (both pons and medulla) and spinal cord, as shown in sagittal sections by antibody staining (Yunker *et al.* 2003), verifying the expression observed in E11.5 hindbrain.

T-type Ca^{2+} channels are expressed more frequently in developing than in mature neurons (Moody & Bosma, 2005), and in those neurons, have been shown to play a role in mediating calcium entry. In some cell lines (neuroblastoma), the expression of T-type Ca^{2+} channels is required for appropriate neurite extension, although this is not observed in all cell lines (for review, see Lory *et al.* 2006). Thalamic neurons, which also express rhythmic pacemaker activity in adult (Contreras, 2006), may depend largely on $Ca_v3.1$; the $Ca_v3.3$ isoform appears when dendritic expansion is occurring, suggesting that the slower kinetics and possible increased Ca^{2+} entry may be involved in that process (Tarasenko *et al.* 1997). Action potential waveform and cloned Ca_v3 channels showed that $Ca_v3.3$ caused sustained Ca^{2+} entry and depolarization in comparison to other Ca_v3 species, perhaps reflecting a developmental and pacemaking role for this channel (Chemin *et al.* 2002).

The differential expression of ion channels involved in initiation and propagation of electrical events in the hindbrain is likely to be developmentally regulated to cause the known window of SA in the hindbrain (E11.5–E13.5; Hunt *et al.* 2006*b*). Although some asynchronous spontaneous activity is observed before E11.5, it is only at that time point that synchronized spontaneous events initiate medially and propagate from the InZ (Gust *et al.* 2003; Hunt *et al.* 2005). A window of SA is not unusual in development of neuronal circuits (see Moody & Bosma, 2005, for review), and may be crucial during a period of axon extension or synapse formation. It is likely that other ion channels subsequently develop that serve to terminate SA. However, at E11.5, the differential expression of $I_{Ca\text{-}T}$ in midline neurons, combined with high resistance, allow long-duration events that propagate into lateral neurons. Serotonergic neurons are among the earliest differentiated group (along with the more lateral motor neurons) in the rostral hindbrain, and thus may acquire the driver role by virtue of that early differentiation.

References

Aghajanian GK & Vandermaelen CP (1982). Intracellular recordings from serotonergic dorsal raphe neurons: pacemaker potentials and the effect of LSD. *Brain Res* **238**, 463–469.

Allene C, Cattani A, Ackman JB, Bonifazi P, Aniksztejn L, Ben-Ari Y & Cossart R (2008). Sequential generation of two distinct synapse-driven network patterns in developing neocortex. *J Neurosci* **28**, 12851–12863.

Bayliss DA, Li YW & Talley EM (1997*a*). Effects of serotonin on caudal raphe neurons: activation of an inwardly rectifying potassium conductance. *J Neurophysiol* **77**, 1349–1361.

Bayliss DA, Li YW & Talley EM (1997*b*). Effects of serotonin on caudel raphe neurons: inhibition of N- and P/Q-type calcium channels and the afterhyperpolarization. *J Neurophysiol* **77**, 1362–1374.

Ben-Ari Y (2001). Developing networks play a similar melody. *Trends Neurosci* **24**, 353–360.

Borodinsky LN, Root CM, Cronin JA, Sann SB, Gu X & Spitzer NC (2004). Activity-dependent homeostatic specification of transmitter expression in embryonic neurons. *Nature* **429**, 523–530.

Burlhis TM & Aghajanian GK (1987). Pacemaker potentials of serotonergic dorsal raphe neurons: contribution of a low-threshold Ca^{2+} conductance. *Synapse* **1**, 582–588.

Chemin J, Nargeot J & Lory P (2002). Neuronal T-type α1H calcium channels induce neuritogenesis and expression of high-voltage-activated calcium channels in the NG108-15 cell line. *J Neurosci* **22**, 6856–6862.

Contreras D (2006). The role of T-channels in the generation of thalamocortical rhythms. *CNS Neurol Disord Drug Targets* **5**, 571–585.

Crepel V, Aronoy D, Jorquera I, Represa A & Ben-Ari Y (2007). A parturition-associated nonsynaptic coherent activity pattern in the developing hippocampus. *Neuron* **54**, 105–120.

Cruikshank SJ, Hopperstad M, Younger M, Connors BW, Spray DC & Srinivas M (2004). Potent block of Cx36 and Cx50 gap junction channels by mefloquine. *Proc Natl Acad Sci U S A* **101**, 12364–12369.

David C, Halliwell J & Whitaker M (1988). Some properties of the membrane currents underlying the fertilization potential in sea urchin eggs. *J Physiol* **402**, 139–154.

Drummond GB (2009). Reporting ethical matters in *The Journal of Physiology*: standards and advice. *J Physiol* **587**, 713–719.

Fuentealba P & Steriade M (2005). The reticular nucleus revisited: intrinsic and network properties of a thalamic pacemaker. *Prog Neurobiol* **75**, 125–140.

Gu X & Spitzer NC (1993). Low-threshold Ca^{2+} current and its role in spontaneous elevations of intracellular Ca^{2+} in developing *Xenopus* neurons. *J Neurosci* **13**, 4936–4948.

Gu X & Spitzer NC (1995). Distinct aspects of neuronal differentiation encoded by frequency of spontaneous Ca^{2+} transients. *Nature* **375**, 784–787.

Gust J, Wright JJ, Pratt EB & Bosma MM (2003). Development of synchronized activity of cranial motor neurons in the segmented embryonic mouse hindbrain. *J Physiol* **550**, 123–133.

Guthrie S (1996). Patterning the hindbrain. *Curr Opin Neurobiol* **6**, 41–48.

Hendricks TJ, Francis N, Fyodorov D & Deneris ES (1999). The ETS domain factor Pet-1 is an early and precise marker of central serotonin neurons and interacts with a conserved element in serotonergic genes. *J Neurosci* **19**, 10348–10356.

Hendricks TJ, Fyodorov DV, Wegman LJ, Lelutiu NB, Pehek EA, Yamamoto B, Silver J, Weeber EJ, Sweatt JD & Deneris ES (2003). Pet-1 ETS gene plays a critical role in 5HT neuron development and is required for normal anxiety-like and aggressive behavior. *Neuron* **37**, 233–247.

Hunt PN, McCabe AK & Bosma MM (2005). Midline serotonergic neurons drive widespread synchronized activity in embryonic mouse hindbrain. *J Physiol* **566**, 807–819.

Hunt PN, Gust J, McCabe AK & Bosma MM (2006*a*). Primary role of the serotonergic midline system in synchronized spontaneous activity during development of the embryonic mouse hindbrain. *J Neurobiol* **66**, 1239–1252.

Hunt PN, McCabe AK, Gust J & Bosma MM (2006*b*). Spatial restriction of spontaneous activity towards the rostral primary initiating zone during development of the embryonic mouse hindbrain. *J Neurobiol* **66**, 1225–1238.

Jacobs BL & Azmitia EC (1992). Structure and function of the brain: serotonin system. *Physiol Rev* **72**, 165–229.

Kirby LG, Pernar L, Valentino RJ & Beck SG (2003). Distinguishing characteristics of serotonin and non-serotonin-containing cells in the dorsal raphe nucleus: electrophysiological and immunohistochemical studies. *Neuroscience* **116**, 669–683.

Lacinová L (2004). Pharmacology of recombinant low-voltage activated calcium channels. *Curr Drug Targets CNS Neurol Disord* **3**, 105–111.

Lee JH, Gomora JC, Cribbs LL & Perez-Reyes E (1999). Nickel block of three cloned T-type calcium channels: low concentrations selectively block α1H. *Biophys J* **77**, 3034–3042.

Lory P, Bidaud E & Chemin J (2006). T-type calcium channels in differentiation and proliferation. *Cell Calcium* **40**, 135–146.

Lumsden A (1990). The cellular basis of segmentation in the developing hindbrain. *Trends Neurosci* **13**, 329–335.

Lumsden A & Keynes R (1989). Segmental patterns of neuronal development in the chick hindbrain. *Nature* **337**, 424–428.

Miljanich GP & Ramachandran J (1995). Antagonists of neuronal calcium channels: structure, function, and therapeutic implications. *Annu Rev Pharmacol Toxicol* **35**, 707–734.

Moody WJ & Bosma MM (2005). Ion channel development, spontaneous activity, and activity-dependent development in nerve and muscle cells. *Physiol Rev* **85**, 883–941.

Nelson MT, Todorovic SM & Perez-Reyes E (2006). The role of T-type calcium channels in epilepsy and pain. *Curr Pharm Des* **12**, 2189–2197.

Okamoto J, Takahashi K & Yamashita E (1977). Ionic currents through the membrane of the mammalian oocyte and their comparison with those in the tunicate and sea urchin. *J Physiol* **267**, 465–495.

Pan ZZ & Williams JT (1994). Muscarine hyperpolarizes a subpopulation of neurons by activating an M2 muscarinic receptor in rat nucleus raphe magnus in vitro. *J Neurosci* **14**, 1332–1338.

Penington JN, Kelly JS & Fox AP (1991). A study of the mechanism of Ca^{2+} current inhibition produced by serotonin in rat dorsal raphe neurons. *J Neurosci* **11**, 3594–3609.

Penington JN, Kelly JS & Fox AP (1992). Action potential waveforms reveal simultaneous changes in I_C and I_K produced by 5-HT in rat dorsal raphe neurons. *Proc Biol Sci* **248**, 171–179.

Penington JN, Kelly JS & Fox AP (1993). Whole-cell recordings of inwardly rectifying K^+ currents activated by 5-HT1A receptors on dorsal raphe neurones of the adult rat. *J Physiol* **469**, 387–405.

Rockhill W, Kirkman JL & Bosma MM (2009). Spontaneous activity in the developing mouse midbrain driven by an external pacemaker. *Dev Neurobiol* **69**, 689–704.

Sun JJ & Luhmann HJ (2007). Spatio-temporal dynamics of oscillatory network activity in the neonatal mouse cerebral cortex. *Eur J Neurosci* **267**, 1995–2004.

Tarasenko AN, Kostyuk PG, Eremin AV & Isaev DS (1997). Two types of low-voltage-activated Ca^{2+} channels in neurons of rat laterodorsal thalamic nucleus. *J Physiol* **499**, 77–86.

Wallace JA & Lauder JM (1983). Development of the serotonergic system in the rat embryo: an immunocytochemical study. *Brain Res Bull* **10**, 459–479.

Watt SD, Gu X, Smith RD & Spitzer NC (2000). Specific frequencies of spontaneous Ca^{2+} transients upregulate GAD 67 transcripts in embryonic spinal neurons. *Mol Cell Neurosci* **16**, 376–387.

Yunker AM, Sharp AH, Sundarraj S, Ranganathan V, Copeland TD & McEnery MW (2003). Immunological characterization of T-type voltage-dependent calcium channel CaV3.1 (alpha 1G) and CaV3.2 (alpha 1I) isoforms reveal differences in their localization, expression, and neural development. *Neurosci.* **117**, 321–335.

Author contributions

All experiments were performed in the Department of Biology at the University of Washington, Seattle WA, USA. A.M.M., N.C.A. and M.M.B. contributed to the conception, design, analysis and interpretation of the data, as well as drafting, revising, and final approval of the article. M.E.H. and J.E.O. contributed to the design of the data, and the drafting and final approval of the article.

Acknowledgements

The authors would like to acknowledge William J. Moody, Jay Conhaim and Jonathan Lischalk for helpful discussions and help with experiments and materials, Glenda Froelick for help with cryosectioning and immunocytochemistry, and Pang Chan for help with confocal use. We thank the National Science Foundation for funding this work.